DOI: 10.1002/ejic.200900968

Luminescence Properties of Redispersible Tb^{3+}-Doped $GdPO_4$ Nanoparticles Prepared by an Ethylene Glycol Route

Ningombam Yaiphaba,[a,b] Raghumani Singh Ningthoujam,*[c] Nongmaithem Rajmuhon Singh,*[a] and Rajesh Kumar Vatsa[c]

Keywords: Lanthanides / Luminescence / Nanoparticles / Dispersion / Polymers

Nanoparticles of Tb^{3+}-doped $GdPO_4$ (Tb^{3+} = 0, 2, 5, 7, 10, and 20 atom-%) have been prepared at a relatively low temperature of 160 °C in ethylene glycol medium. The particles crystallize in a monoclinic structure with an average crystallite size of 30–50 nm. From the luminescence study of Tb^{3+}-doped $GdPO_4$, the magnetic dipole transition ($^5D_4 \rightarrow {}^7F_5$) at 545 nm (green) was found to be more prominent than the electric dipole transition ($^5D_4 \rightarrow {}^7F_6$) at 484 nm (blue). Maximum luminescence intensity and lifetime was observed for 7 atom-% Tb^{3+}. Above 7 atom-% Tb^{3+}, a decrease in luminescence was observed. This has been attributed to a concentration-quenching effect due to the cross-relaxation among Tb^{3+} ions. The highest luminescence intensity of Tb^{3+} was observed after excitation at 274 nm ($^8S_{7/2} \rightarrow {}^6I_{11/2}$ of Gd^{3+}) among various excitation wavelengths (including f–f absorptions of Tb^{3+}). This is due to an efficient transfer of energy from Gd^{3+} to Tb^{3+} that shows $GdPO_4$ to be a potential host for Tb^{3+}. These nanoparticles are found to be redispersible in water and ethanol and are incorporated into polyvinyl alcohol film homogeneously. This film showed bright green emission.

Introduction

In recent years, nanoscience and nanotechnology have grown explosively because of the increasing availability of preparation methods of nanomaterials as well as advanced tools of characterization and manipulation. In this regard, luminescent nanomaterials doped with rare-earth ions are of immense importance because of their technological applications in lighting, displays, X-ray photography, lasers, and amplifiers for fiberoptic communication.[1–5] Phosphor materials in nanoparticle form have many advantages over the larger or micron-sized particles. It has been found that phosphor materials such as Y_2O_3:Eu^{3+} in nanoparticle form have a higher luminescence of Eu^{3+} relative to their bulk counterparts under UV excitation (260 nm). This is related to an increase in the band gap with a decrease in the particle size of the host (Y^{3+}–O^2) and thereby an increase in the absorption cross-section for nanoparticles.[6] Energy transfer from the host (Y^{3+}–O^2) to Eu^{3+} is greater for nanoparticles than that for the bulk. However, the peak position of Eu^{3+} emission does not change owing to pure electronic transitions. Due to this reason, extensive studies on nanoparticles doped with lanthanide ions have been reported.[7,8] These nanomaterials are suitable for luminescence detection in bioassays due to their excellent spectral characteristics such as narrow line-shaped emission bands, large stokes shifts, long-lived luminescence, and inherent photostability.

Phosphates of Ln^{3+} (Ln^{3+} = Y^{3+}, La^{3+}, Gd^{3+}, Lu^{3+}) are good hosts for other activator Ln^{3+} ions because of the following characteristics: maximum transparency in the visible spectral region, high thermal, chemical, and mechanical stability, and a cutoff frequency up to 1100 cm^{-1} ($LnPO_4$).[9,10] Li and his group[11] prepared uniform $LnPO_4 \cdot xH_2O$ (Ln = Y, La–Nd, Sm–Lu) nanocrystals that have controlled 0D, 1D, and 2D structures and concluded that the optical properties of these nanocrystals are strongly dependent on their morphological properties. A variety of methods have been developed to synthesize Tb^{3+}-doped $LnPO_4$. Kömpe et al.[12] prepared $CePO_4$:Tb^{3+} core and core–shell nanoparticles by the coprecipitation method using coordinating ligands like tributyl phosphate (TBP) and trihexylamine in a water-free environment at 200 °C. Stouwdam et al.[13] have also prepared surface-coated nanoparticles of LaF_3 and $LaPO_4$ doped with the luminescent trivalent lanthanide ions Eu^{3+}, Nd^{3+}, Er^{3+}, Pr^{3+}, Ho^{3+}, and Yb^{3+} by chemical methods. Bühler and Feldmann[14] synthesized luminescent $LaPO_4$:Ce,Tb nanoparticles with a high quantum yield using a microwave-assisted synthesis method with ionic liquid as the reaction media. Many extensive works on $LnPO_4$ doped with activators have been reported in an attempt to understand particle size and shape dependence on chemical and physical properties.[15–20] However, it is desirable to prepare nanoparticles

[a] Department of Chemistry, Manipur University, Canchipur, Imphal, Manipur 795003, India
E-mail: rajmuhon@yahoo.co.in
[b] Department of Chemistry, United College, Chandel, Manipur 795127, India
[c] Chemistry Division, Bhabha Atomic Research Centre, Trombay, Mumbai 400085, India
E-mail: rsn@barc.gov.in

of such phosphors at relatively low temperatures so that significant reduction in both the particle aggregation and segregation of lanthanide ions (e.g., Ln_2O_3, where Ln = Eu, Tb, Dy activators) can be achieved. During low-temperature synthesis, the organic ligands can stabilize the nanoparticles at the synthesis temperature, thereby preparing them for incorporation into polymer-/sol–gel-based luminescent and display devices.

The present study deals with the low-temperature synthesis and luminescence properties of Tb^{3+}-doped $GdPO_4$ nanoparticles using ethylene glycol as solvent. Low-temperature synthesis using ethylene glycol helps to stabilize the nanoparticles and thereby prevent their aggregation after nucleation, without using any moisture-sensitive reagents, hydrothermal conditions, and long-chain organic molecules as stabilizing ligands. These stabilized nanoparticles are dispersible in aqueous/organic solvents (water and ethanol), thereby allowing for the development of polymer/sol–gel-based luminescent materials. The dispersed particles are incorporated into polyvinyl alcohol to get a polymer film.

Results and Discussion

XRD Study

The X-ray diffraction (XRD) patterns of as-prepared Tb^{3+}-doped $GdPO_4$ (Tb^{3+} = 2, 7, and 10 atom-%) are given in Figure 1. The particles crystallize in a monoclinic $GdPO_4$ structure. The average crystallite sizes were calculated using the Debye–Scherrer equation ($d = 0.9\lambda/B\cos\theta$) and were found to be in the range of 33–50 nm for all Tb^{3+}-doped samples. Here, particles are assumed to be spherical in shape and their diameter is considered to be the crystallite size. The unit-cell parameters were calculated using the following relation between Bragg diffraction spacing and monoclinic cell parameters.[21] The lattice parameters for pure $GdPO_4$ are a = 6.667(1) Å, b = 6.843(1) Å, c = 6.335(1) Å, and its unit-cell volume is 279.87 Å^3. The lattice parameters for 7 atom-% Tb^{3+}-doped $GdPO_4$ are a = 6.629(1) Å, b = 6.873(1) Å, c = 6.325(1) Å, and its unit-cell volume is 279.5 Å^3. Figure 2 shows the plot of unit-cell volume versus Tb^{3+} concentration. Unit-cell volume decreases with increasing Tb^{3+} concentration due to the difference in ionic radii of Tb^{3+} (1.04 Å) and Gd^{3+} (1.06 Å).[22] These results show the substitution of the Tb^{3+} ions into the Gd^{3+} sites of $GdPO_4$.

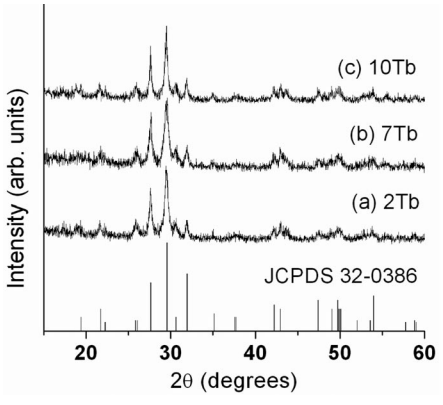

Figure 1. XRD patterns of $GdPO_4$:Tb^{3+} nanoparticles: (a) 2, (b) 7, and (c) 10 atom-% Tb^{3+}. The standard pattern of the monoclinic phase is also included.

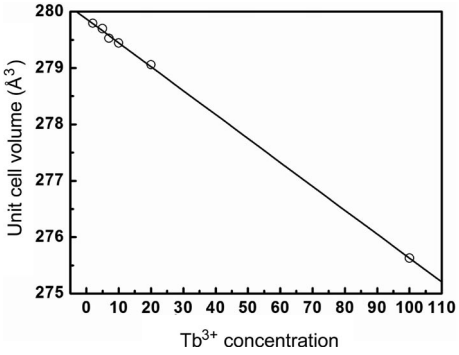

Figure 2. Plot of unit-cell volume versus Tb^{3+} concentration in the as-prepared Tb^{3+}-doped $GdPO_4$ (Tb^{3+} = 2, 5, 7, 10, and 20 atom-%) nanoparticles.

IR and Morphology Studies

The IR spectrum of 2 atom-% Tb-doped $GdPO_4$ nanoparticles is shown in Figure 3. Prominent peaks at 551, 572, 628, 885, 946, 1070, 1460, 1662, 2856, 2927, and 3310 cm^{-1} are observed. Based on $(PO_4)^{3-}$ group symmetry, band regions are defined as $\tilde{\nu}_1$, $\tilde{\nu}_2$, $\tilde{\nu}_3$, and $\tilde{\nu}_4$, respectively.[17,18] Band regions $\tilde{\nu}_1$ and $\tilde{\nu}_2$ are due to Raman active modes, whereas $\tilde{\nu}_3$ and $\tilde{\nu}_4$ are due to IR active modes and correspond to the stretching and bending vibrations. The bending vibrations of $(PO_4)^{3-}$, which are considered as the $\tilde{\nu}_4$ region, have been assigned at 551, 572, and 628 cm^{-1}.[23,24] The stretching vibrations of $(PO_4)^{3-}$, which are referred to as the $\tilde{\nu}_3$ region, have been assigned at 885, 946, and 1070 cm^{-1}.[23,24] In previous studies on $LnPO_4$ (Ln = Gd, Y, La),[24–29] similar peaks were reported. Peaks at 1662 and 3310 cm^{-1} correspond to bending and stretching vibrations, respectively, for the O–H group of the ethylene glycol molecule, which is used as a capping agent for nanoparticles.[27,29–32] However, free O–H has a stretching frequency at 3650 cm^{-1}.[23] The broad band at 3310 cm^{-1} therefore indicates the presence of a hydrogen bond in ethylene glycol molecules. Water associated with $GdPO_4$ could not be distinguished because the O–H peaks due to water have been merged with those of ethylene glycol. The wagging vibration at 1266 cm^{-1}, twisting vibration at 1155 cm^{-1}, and rocking vibration at 899 cm^{-1} due to the presence of CH_2 from ethylene glycol have been merged with bands of $(PO_4)^{3-}$. The peaks at 2856 and 2927 cm^{-1} correspond to the stretching vibrations of the CH_2 group of the ethylene glycol molecule, whereas its bending vibration (scissoring) is observed at 1460 cm^{-1}.[27,29–32] The peak at 2362 cm^{-1} is

due to absorption of CO_2 gas from the atmosphere on the surface of particles. The IR study suggests the presence of ethylene glycol along with nanoparticles and thus will help in the incorporation of nanoparticles in polar media.

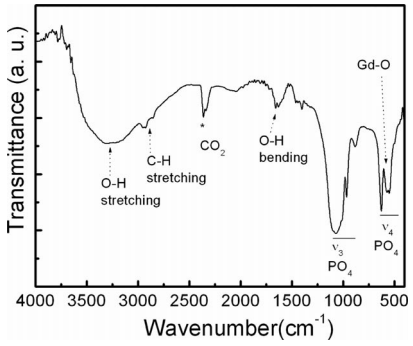

Figure 3. IR spectrum of 2 atom-% Tb^{3+}-doped $GdPO_4$.

Figure 4 (a–c) shows the simple photographic images of powder of 7 atom-% Tb-doped $GdPO_4$, dispersion of powder in ethanol, and its film after the incorporation of dispersed powder into polyvinyl alcohol. There is a homogeneous dispersion of powder in ethanol (Figure 4, b). Also, Figure 4 (c) shows the homogeneity distribution of particles in polymer after the incorporation of dispersed powder. A TEM image of the 2 atom-% Tb^{3+}-doped $GdPO_4$ after dispersion in ethanol is shown in Figure 4 (d); there are nanorods with a diameter of 20–30 nm and lengths of 100–200 nm. It was further characterized by selected-area electron diffraction (SAED). The diffraction rings are clearly visible, thereby proving the crystallinity of the samples.

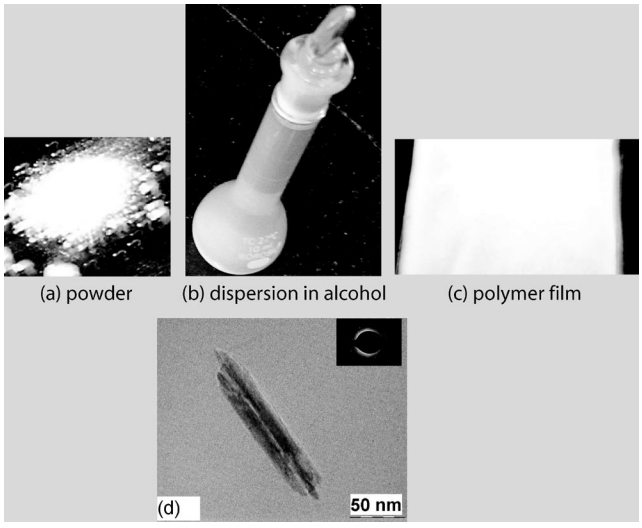

Figure 4. $GdPO_4$ sample doped with 7 atom-% Tb^{3+}: sample images of (a) powder, (b) dispersion of powder in ethanol, and (c) polyvinyl alcohol film after incorporation of dispersed powder. (d) TEM image of powder after dispersion in ethanol. The inset shows its selected-area electron diffraction.

Luminescence Study

Figure 5 shows the excitation spectrum of 7 atom-% Tb^{3+}-doped $GdPO_4$ with a monitoring emission at 545 nm. Here, a 495 nm filter was used. The spectrum consists of many sharp peaks at 274, 312, 352, 368, and 378 nm. The peak at 274 nm corresponds to the $^8S_{7/2} \rightarrow {}^6I_{11/2}$ transition of Gd^{3+},[31] and this peak has the highest absorption relative to the others. It indicates the occurrence of an energy-transfer process from the Gd^{3+} to the Tb^{3+} ion. The remaining peaks [i.e., $^7F_6 \rightarrow {}^5L_9$ (312 nm), $^7F_6 \rightarrow {}^5G_5$ (352 nm), $^7F_6 \rightarrow {}^5L_{10}$ (368 nm), and $^7F_6 \rightarrow {}^5G_6$ (378 nm)] correspond to the 4f–4f transitions of Tb^{3+}.[33] It is to be noted that the second harmonic generation of 545 nm will give approximately 273 nm. To check it, we carried out another excitation spectrum of 2 atom-% Tb^{3+}-doped $GdPO_4$ with a monitoring emission at 488 nm and a 395 nm filter (not shown). In this case, the second harmonic generation of 488 nm will give a peak at 244 nm, but it is not observed. Still, the same excitation-peak position at 274 nm was obtained. It confirms that the excitation peak at 274 nm is genuine.

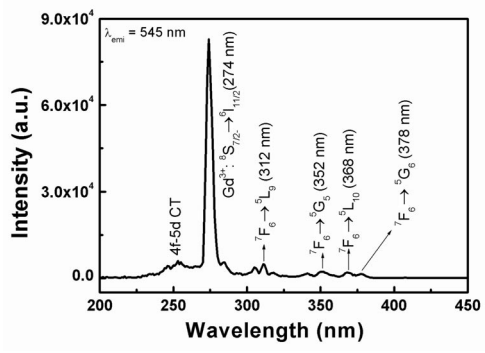

Figure 5. Excitation spectrum of 7 atom-% Tb^{3+}-doped $GdPO_4$ monitored at 545 nm emission.

Figure 6 shows the emission spectra of 7 atom-% Tb^{3+}-doped $GdPO_4$ at different excitation wavelengths of 274, 312, and 352 nm. The 395 nm filter was used. Several emission lines at 489, 545, 587, and 621 nm were observed in the spectra, and the peaks correspond to $^5D_4 \rightarrow {}^7F_6$ (489 nm), $^5D_4 \rightarrow {}^7F_5$ (545 nm), $^5D_4 \rightarrow {}^7F_4$ (587 nm), and $^5D_4 \rightarrow {}^7F_3$ (621 nm) transitions of Tb^{3+}, respectively.[11,12,14] Maximum emission intensity was observed after excitation at 274 nm, followed by 320 and 350 nm. The strongest emission was obtained at 545 nm, thus giving rise to the green emission for Tb^{3+}. The peaks at 489 and 545 nm correspond to the electric-dipole- and magnetic-dipole-allowed transitions, respectively.

To see changes in emission intensity for different concentrations of Tb^{3+}, emission spectra of Tb^{3+}-doped $GdPO_4$ (Tb^{3+} = 2, 5, 7, 10 atom-%) were recorded after excitation at 274 nm (Figure 7). All the samples show similar spectral patterns. To compare all samples, the integrated area for the

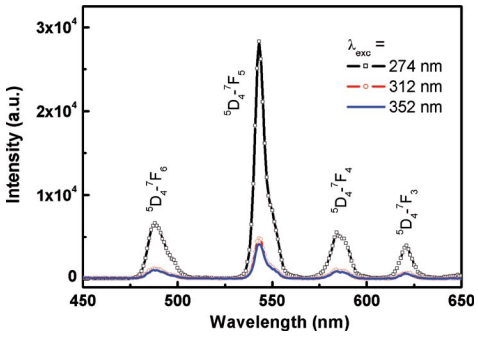

Figure 6. Emission spectra of 7 atom-% Tb^{3+}-doped $GdPO_4$ after excitation at 274, 312, and 352 nm.

$^5D_4 \rightarrow {}^7F_5$ transition in the range 530–560 nm was calculated. The integrated area for the $^5D_4 \rightarrow {}^7F_5$ transition of Tb^{3+}-doped $GdPO_4$ as a function of Tb^{3+} concentration is shown in Figure 8. Emission intensity increases as Tb^{3+} concentration increases from 2 to 7 atom-% and then decreases with a further increase of Tb^{3+}. The decrease in the intensity with increasing Tb^{3+}-ion concentration is due to the concentration-quenching effect.[3]

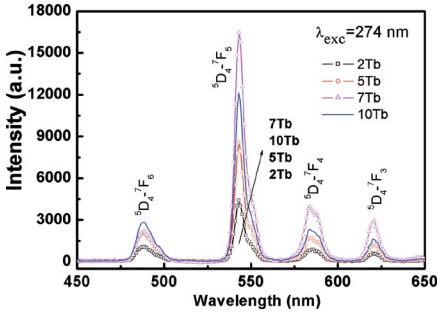

Figure 7. Emission spectra of 2, 5, 7, and 10 atom-% Tb^{3+}-doped $GdPO_4$ after excitation at 274 nm.

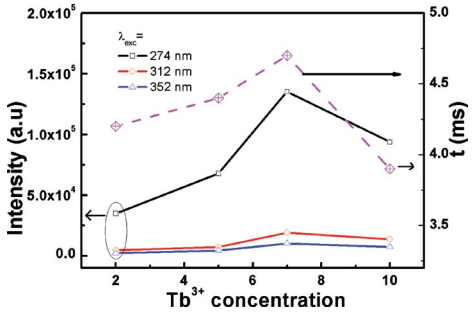

Figure 8. Integrated area (intensity) under the $^5D_4 \rightarrow {}^7F_5$ peak (left side) and decay lifetime (right side) for the $^5D_4$ level versus Tb^{3+} concentration in as-prepared Tb^{3+}-doped $GdPO_4$ nanoparticles. The samples were excited at 274, 312, and 352 nm.

Lifetime Study

Figure 9 shows the luminescent decays for the $^5D_4$ level of Tb^{3+} at room temperature in $GdPO_4$:Tb^{3+} (Tb^{3+} = 2, 5, 7, 10, 20 atom-%) after excitation at 274 nm. Their ln(*I*) versus time plots are shown in the inset of Figure 9. Here, *I* stands for luminescence intensity. It was found that each set of data does not show a straight line. Decay data were fitted with both monoexponential and biexponential equations. The monoexponential decay fit is expressed as Equation (1).

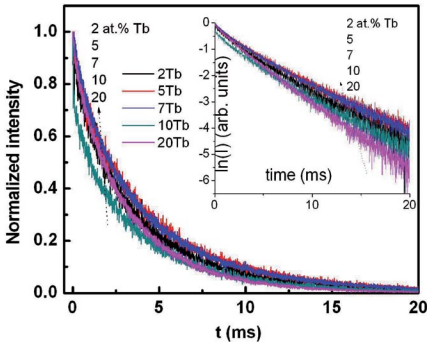

Figure 9. Decay curves for the $^5D_4$ level of Tb^{3+} for Tb^{3+}-doped $GdPO_4$ (Tb^{3+} = 2, 5, 7, 10, 20 atom-%). The excitation wavelength was fixed at 274 nm. The arrow indicates the variation of intensity with Tb (atom-%). The inset shows their ln(*I*) versus time plots. The arrow indicates the trend of increasing Tb^{3+} percentage concentrations.

$$I = I_0 \exp(-t/\tau) \quad (1)$$

where I_0 and I are intensities at zero time and at time t, respectively, and τ is the lifetime for the transition. This was carried out by considering the following assumptions:[10,12,34–37] (i) the homogeneous distribution of Tb^{3+} ions in the host matrix, and (ii) Tb^{3+} ions may be located closer to the surface due to a strong ligand–Tb^{3+} interaction and a strong quenching effect at higher concentrations. And the second-order exponential decay is given as Equation (2).

$$I = I_1 \exp(-t/\tau_1) + I_2 \exp(-t/\tau_2) \quad (2)$$

where I_1 and I_2 are intensities at two different interval times and the corresponding decay times are τ_1 and τ_2. The $\tau_{average}$ is calculated using the following equation [Equation (3)].[10,12,34–37]

$$\tau_{average} = (I_1\tau_1 + I_2\tau_2)/(I_1 + I_2) \quad (3)$$

The possibilities of such biexponential decay are[10,12,34–37] (i) a difference in the nonradiative probability of decays for lanthanide ions at or near the surface and in the core of the particles, (ii) an inhomogeneous distribution of the dopant ions in the host material, which leads to the variation in the local concentrations, and (iii) the transfer of excitation energy from donor to lanthanide activators. Of the two exponential fits, we observed a better fit with the biexponential equation than with the monoexponential one (Figure 10), that is, the goodness of fits of parameters for 7 atom-% Tb-doped $GdPO_4$ with mono- and biexponential equations were found to be 0.9916 and 0.9979, respectively. As the concentration of Tb^{3+} in Tb^{3+}-doped $GdPO_4$ increases above 7 atom-%, the lifetime decreases (Figure 8). This behavior is attributed to strong quenching because the distance between the Tb^{3+}–Tb^{3+} decreases.[3]

Moreover, cross-relaxation among the Tb^{3+} ions is dominant over the nonradiative relaxation, which arises from the surface or near the surface for higher-doped samples. The lifetimes vary from 3.9 to 4.7 ms for Tb^{3+}-doped $GdPO_4$ nanoparticles (Tb^{3+} = 2, 5, 7, 10 atom-%).

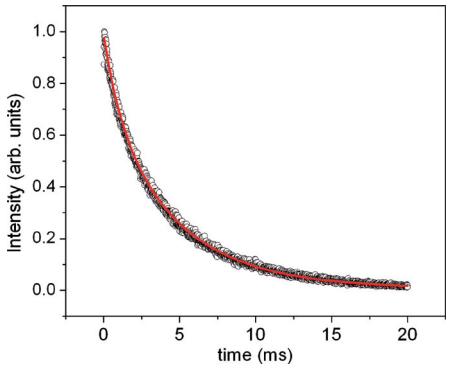

Figure 10. Decay curve for the $^5D_4$ level of Tb^{3+} for 7 atom-% Tb^{3+}-doped $GdPO_4$; the excitation wavelength is fixed at 274 nm. The line was fit to the data using the biexponential decay equation.

Dispersion of Particles in Polar Media

The emission spectra of 7 atom-% Tb^{3+}-doped $GdPO_4$ samples were also studied by redispersing the material in water (Figure 11) and ethanol (not shown). In both water and ethanol, the f–f transitions of Tb^{3+} are easily observed, and the intensity of the $^5D_4 \rightarrow {}^7F_5$ transition is found to be highest. The redispersion of the as-prepared Tb^{3+}-doped $GdPO_4$ nanoparticles in water and ethanol are due to capping by the ethylene glycol on the surface of the nanoparticles, as confirmed by IR spectroscopy studies. Further, we were able to incorporate dispersible nanoparticles into a polymer (polyvinyl alcohol) film (about 0.5 mm thickness and ca. 10×10 mm^2). The film is homogeneous and shows green luminescence after excitation at 274 nm, which is shown in Figure 12. However, the emission intensity is less than the powder one of Figure 6 because the amount of Eu^{3+} activator per volume is less for the film relative to that for the original powder. Both the excitation spectrum (left) and the decay for the $^5D_4$ level of Tb^{3+} (right) are shown as insets of Figure 12. Interestingly, the decay is monoexponential with a lifetime of 3.4 ms. Such monoexponential decay suggests the homogeneous distribution of Tb^{3+} ions. This film has the potential to be useful in optical devices.

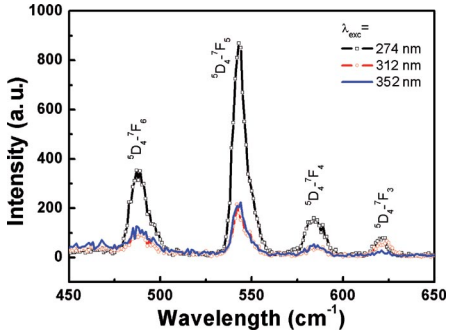

Figure 11. Emission spectra of 7 atom-% Tb^{3+}-doped $GdPO_4$ dispersed in water after different excitations.

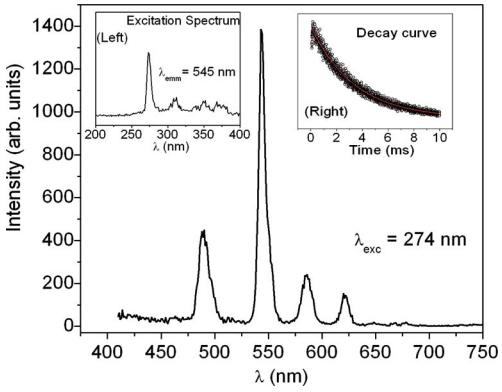

Figure 12. Emission spectra of polymer film after incorporating the dispersed 7 atom-% Tb^{3+}-doped $GdPO_4$ in water in polyvinyl alcohol after excitation at 274 nm. Inset: left and right show the corresponding excitation spectrum and luminescence decay, respectively.

Conclusion

Tb^{3+}-doped $GdPO_4$ nanoparticles were synthesized and their luminescence properties have been investigated. For the different excitation wavelengths, the most prominent emission was observed at 274 nm excitation, thereby showing an efficient energy transfer from Gd^{3+} to Tb^{3+}. The luminescence intensity increases up to 7 atom-% Tb^{3+} and then decreases as the dopant concentration of Tb^{3+} increases. This has been attributed to the concentration-quenching effect. Moreover, the as-prepared Tb^{3+}-doped $GdPO_4$ nanoparticles were redispersible in water and ethanol, thus making them a potential target for biological labeling. Such nanoparticles can be incorporated into polyvinyl alcohol polymer, and this film has the potential to be useful in optical devices.

Experimental Section

Preparation: Tb^{3+}-doped $GdPO_4$ (Tb^{3+} = 2, 5, 7, 10, and 20 atom-%) was prepared by the coprecipitation method in ethylene glycol at 160 °C. For the preparation of 2 atom-% Tb^{3+}, Gd_2O_3 (500 mg; 99.99%, Aldrich) and $TbNO_3$ (10 mg; 99.99%, Aldrich) were dissolved in a minimum quantity of dilute HCl to get a clear solution. An excess amount of HCl acid was removed by evaporation with distilled water. Chlorides of Gd^{3+} and Tb^{3+} thus formed were mixed with $(NH_4)H_2PO_4$ (0.3340 g; 99.99%, Aldrich) dissolved in a minimum amount of distilled water. To this, ethylene glycol (50 mL) was added and heated for 3 h at 160 °C. The white precipitates that appeared were separated by centrifugation, washed repeatedly with ethanol and acetone to remove excess amounts of ethylene glycol, and dried under ambient conditions.

Characterization: X-ray diffraction (XRD) measurements were carried out with a Philips powder X-ray diffractometer (model PW 1071) with Ni-filtered Cu-K_α radiation. The lattice parameters were calculated from the least-square fitting of the diffraction

peaks. The crystallite size (d) was calculated from the diffraction line width based on the Scherrer relation: $d = 0.9\lambda/B\cos\theta$, where λ is the wavelength of X-rays and B is the full width at half-maximum.

The infrared (IR) spectrum of the $GdPO_4$ sample was recorded with a Bomem (MB102-Series) Fourier transform infrared spectrometer.

The transmission electron microscopy (TEM) images were recorded with a JEM 2000 FX instrument (JEOL Make). A powder sample (about 5 mg) was mixed with glycerin (10 mL) and dispersed under ultrasonic vibration for 1 h. A drop of the dispersed particles was put over the carbon-coated Cu grid, was evaporated using a lamp, and was finally mounted inside the sample chamber.

The excitation and emission spectra were recorded with an Edinburgh Instruments (model F900) fluorescence spectrometer with a 450-W Xe lamp as the excitation source. A Nd:YAG laser-pumped optical parametric oscillator (OPO) with a pulse width of 10 ns and a repetition frequency of 10 Hz was used as the excitation source for recording decay lifetimes and the intensity of decay was recorded using the Edinburgh Instruments fluorescence spectrometer.

Powder samples (5 mg) were mixed with methanol, spread over a quartz plate, dried in an ambient atmosphere, and mounted inside the sample chamber. The luminescence data was analyzed using Origin 6.1 software.

Acknowledgments

The authors acknowledge Dr. T. Mukherjee (Chemistry Group) and Dr. D. Das (Chemistry Division) of BARC for their encouragement during this work. The authors especially like to thank Dr. M. Kumar, RPCD, BARC for his help in making polymer film. Two of the authors, N. R. S. and N. Y., acknowledge the Council of Scientific and Industrial Research (CSIR), New Delhi and Manipur University for providing financial support during the execution of this work.

[1] K. Riwotzki, H. Meyssamy, H. Schnablegger, A. Kornowski, M. Hasse, *Angew. Chem. Int. Ed.* **2001**, *40*, 573–576.
[2] J. C. Park, H. K. Moon, D. K. Kim, S. H. Byeon, B. C. Kim, K. S. Suh, *Appl. Phys. Lett.* **2000**, *77*, 2162–2164.
[3] G. Blasse, B. C. Grabmaier, *Luminescent Materials*, Springer-Verlag, Berlin, **1994**.
[4] J. R. O'Connor, *Appl. Phys. Lett.* **1966**, *9*, 407–409.
[5] D. B. Barber, C. R. Pollock, L. L. Beecroft, C. K. Ober, *Opt. Lett.* **1997**, *22*, 1247–1249.
[6] J. Dhanaraj, R. Jagannathan, T. R. N. Kutty, C.-H. Lu, *J. Phys. Chem. B* **2001**, *105*, 11098–11105.
[7] E. M. Goldys, K. Drozdowicz-Tomsia, S. Jinjun, D. Dosev, I. M. Kennedy, S. Yatsunenko, M. Godlewski, *J. Am. Chem. Soc.* **2006**, *128*, 14498–14505.
[8] K. Riwotzki, H. Meyssamy, A. Kornowski, M. Haase, *J. Phys. Chem. B* **2000**, *104*, 2824–2828.
[9] a) U. Rambabu, N. R. Munirathnam, T. L. Prakash, S. Buddhudu, *Mater. Chem. Phys.* **2002**, *78*, 160–169; b) N. Rakov, G. S. Maciel, *J. Lumin.* **2007**, *126*, 703–706.
[10] J. W. Stouwdam, F. C. J. M. van Veggel, *Nano Lett.* **2002**, *2*, 733–737.
[11] a) R. Yan, X. Sun, X. Wang, Q. Peng, Y. Li, *Chem. Eur. J.* **2005**, *11*, 2183–2195; b) Z. Huo, C. Chen, D. Chu, H. Li, Y. Li, *Chem. Eur. J.* **2007**, *13*, 7708–7714.
[12] K. Kömpe, H. Borchert, J. Storz, A. Lobo, S. Adam, T. Möller, M. Haase, *Angew. Chem. Int. Ed.* **2003**, *42*, 5513–5516.
[13] J. W. Stouwdam, G. A. Hebbink, J. Huskes, F. C. J. M. van Veggel, *Chem. Mater.* **2003**, *15*, 4604–4616.
[14] G. Bühler, C. Feldmann, *Angew. Chem. Int. Ed.* **2006**, *45*, 4864–4867.
[15] S. Heer, O. Lehmann, M. Haase, H.-U. Güdel, *Angew. Chem. Int. Ed.* **2003**, *42*, 3179–3182.
[16] O. Lehmann, H. Meyssamy, K. Kömpe, H. Schnablegger, M. Haase, *J. Phys. Chem. B* **2003**, *107*, 7449–7453.
[17] H.-X. Mai, Y.-W. Zhang, L.-D. Sun, C.-H. Yan, *Chem. Mater.* **2007**, *19*, 4514–4522.
[18] C.-H. Yan, L.-D. Sun, C.-S. Liao, Y.-X. Zhang, Y.-Q. Lu, S.-H. Huang, S.-Z. Lü, *Appl. Phys. Lett.* **2003**, *82*, 3511.
[19] Z. Huo, C. Chen, Y. Li, *Chem. Commun.* **2006**, 3522–3524.
[20] J. Bao, R. Yu, J. Zhang, X. Yang, D. Wang, J. Deng, J. Chen, X. Xing, *Eur. J. Inorg. Chem.* **2009**, *2388*, 2388–2392.
[21] B. D. Cullity, *Elements of X-ray Diffraction*, Addision-Wesley, Reading, MA, USA, **1959**.
[22] R. D. Shannon, C. T. Prewitt, *Acta Crystallogr., Sect.* ***B*** **1969**, *25*, 925–946.
[23] M. Ferhi, K. Horchani-Naifer, M. Férid, *J. Rare Earths* **2009**, *27*, 182–186.
[24] G. M. Begun, G. W. Beall, L. A. Boatner, W. J. Gregor, *J. Raman Spectrosc.* **1981**, *11*, 273–278.
[25] S. Lucas, E. Champion, D. Bernache-Assollant, G. Leroy, *J. Solid State Chem.* **2004**, *177*, 1312–1320.
[26] Z. Huo, C. Chen, D. Chu, H. Li, Y. Li, *Chem. Eur. J.* **2007**, *13*, 7708–7714.
[27] K. Nakamoto, *Infrared and Raman Spectra of Inorganic and Coordination Compounds*, 5th ed., Wiley, New York, USA, **1986**.
[28] S. Gallini, J. R. Jurado, M. T. Colomer, *Chem. Mater.* **2005**, *17*, 4154–4161.
[29] W. Kemp, *Organic Spectroscopy*, 2nd ed., Macmillan, Hampshire, UK, **1975**.
[30] R. S. Ningthoujam, N. S. Gajbhiye, A. Ahmed, S. S. Umre, S. J. Sharma, *J. Nanosci. Nanotechnol.* **2008**, *8*, 3059–3062.
[31] N. S. Gajbhiye, R. S. Ningthoujam, A. Ahmed, D. K. Panda, S. S. Umre, S. J. Sharma, *Pramana* **2008**, *70*, 313–321.
[32] R. S. Ningthoujam, V. Sudarshan, S. K. Kulshreshtha, *J. Lumin.* **2007**, *127*, 747–756.
[33] S. L. Ng, Y. L. Lam, Y. Zhou, B. S. Ool, C. H. Kam, K. S. Wong, U. Rambabu, S. Buddhudu, *J. Mater. Sci. Lett.* **2000**, *19*, 495–497.
[34] R. S. Ningthoujam, R. Shukla, R. K. Vatsa, V. Duppel, L. Kienle, A. K. Tyagi, *J. Appl. Phys.* **2009**, *105*, 084304–7.
[35] N. S. Singh, R. S. Ningthoujam, L. R. Devi, N. Yaiphaba, V. Sudarsan, S. D. Singh, R. K. Vatsa, R. Tewari, *J. Appl. Phys.* **2008**, *104*, 104307–9.
[36] N. S. Singh, R. S. Ningthoujam, N. Yaiphaba, R. K. Vatsa, S. D. Singh, *J. Appl. Phys.* **2009**, *105*, 064303–7.
[37] N. Yaiphaba, R. S. Ningthoujam, N. S. Singh, R. K. Vatsa, N. R. Singh, *J. Lumin.* **2010**, *130*, 174–180.

Received: September 29, 2009
Published Online: January 19, 2010

